A. SHILNIKOV
Department of Mathematics and Statistics
Georgia State University
Atlanta, GA 30303, USA
E-mail: ashilnikov@gsu.edu

G. CYMBALYUK
Department of Physics and Astronomy
Georgia State University
Atlanta, GA 30303, USA
E-mail: gcym@phy-astr.gsu.edu

HOMOCLINIC BIFURCATIONS OF PERIODIC ORBITS EN A ROUTE FROM TONIC-SPIKING TO BURSTING IN NEURON MODELS

Received August 19, 2004 DOI: 10.1070/RD2004v009n03ABEH000281

The methods of qualitative theory of slow-fast systems applied to biophysically realistic neuron models can describe basic scenarios of how these regimes of activity can be generated and transitions between them can be made. We demonstrate how two different codimension-one bifurcations of a saddle-node periodic orbit with homoclinic orbits can explain transitions between tonic spiking and bursting activities in neuron models following Hodgkin-Huxley formalism. In the first case, we argue that the Lukyanov-Shilnikov bifurcation of a saddle-node periodic orbit with non-central homoclinics is behind the phenomena of bi-stability observed in a model of a leech heart interneuron under defined pharmacological conditions. This model can exhibit two coexisting types of oscillations: tonic spiking and bursting. Moreover, the neuron model can also generate weakly chaotic trains of bursting when a control parameter is close to the bifurcation value. In the second case, the transition is continuous and reversible due to the blue sky catastrophe bifurcation. This bifurcation provides a plausible mechanism for the regulation of the burst duration which may increases with no bound as $1/\sqrt{\alpha - \alpha_0}$, where α_0 is the transitional value, while the inter-burst interval remains nearly constant.

1. Introduction

Stable periodic orbits have a very special role in nonlinear dynamics, and in computational neuroscience in particular, where their topology is associated with specific, regular activities of neurons such as tonic spiking and bursting.

Various patterns of bursting activities have been described in terms of the qualitative theory of slow-fast systems [1, 2, 3, 4]. The classification of routes describing possible transitions between tonic spiking and bursting activities is yet incomplete and remains a fundamental problem for both neuroscience and the theory of dynamical systems [5, 6, 7, 8, 9, 10]. Qualitative description of a transition yields quantitative information about changes of certain physical characteristics associated with the transition. This approach has proven exemplary in neuroscience for studies of transitions between silence and tonic-spiking activities. Applications of qualitative theory of slow-fast dynamical systems to identification of transitions between tonic spiking and bursting can provide vital information about the neuronal activity.

Some transitions are associated with the chaotic behavior, which is due to the shift dynamics arising near a homoclinic bifurcation of a saddle (or saddle-focus) point of a singularly perturbed system [8, 11]. One of such routes can be singled out by the following chain of bifurcations as a control

Mathematics Subject Classification 37C25, 37C27, 37C70, 37N25, 34C26, 34C37, 34C29

parameter is varied; namely, the periodic spiking undergoes a series of period-doubling bifurcations followed by a homoclinic bifurcation of a saddle equilibrium [8, 9]. Terman [8] gives a rigorous proof of the existence of Smale horseshoes in this case, so chaos is a key signature for transitions of this kind.

In this paper, we describe two novel, distinct mechanisms of the transition. Both are based on a saddle-node bifurcation for periodic orbits with homoclinics orbits [12, 13]. Locally, either bifurcation is of codimension one, i.e. the bifurcating saddle-node periodic orbit has a single multiplier equal to +1. What make the bifurcation different is the global behavior of the unstable manifold which becomes homoclinic, i.e. bi-asymptotic to the periodic orbit in both forward and backward time. The feature of the first case is that homoclinic orbits to the saddle-node orbit are not central [14], i.e. they come back to the bifurcating periodic orbit L_{sn} transversally to its strongly stable manifold W^u, as shown in Fig. 1.

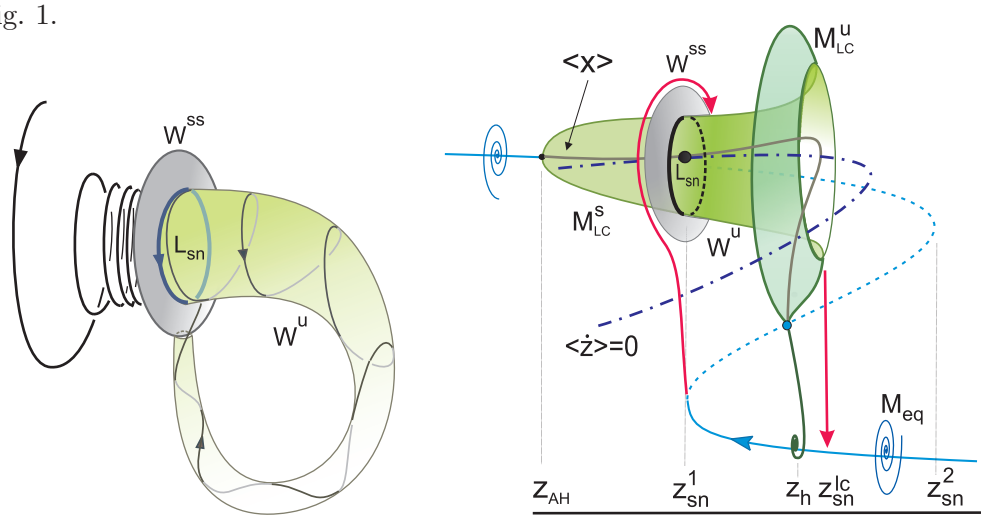

Fig. 1. Saddle-node periodic orbit L_{sn} with noncentral homoclinics: the unstable manifold W^u comes back to L_{sn} crossing transversally the non-leading manifold W^{ss}. The later separates the node region (from the right of W^{ss}) where the periodic orbit L_{sn} is stable from the saddle region containing the unstable manifold W^u comprised of the trajectories converging to L_{sn} as time tends to $-\infty$. (b) Same bifurcation in the singularly perturbed system (3.1): tangency between the nullclines $\langle \dot{z} \rangle = 0$ and $\langle x \rangle$ makes a saddle-node periodic orbit L_{sn}. See description in the sections below.

At this bifurcation, a stable periodic orbit representing tonic spiking merges with a saddle periodic orbit having transverse homoclinic trajectories. This mechanism is distinguished by a bi-stability in the system such that either tonic spiking or bursting (periodic and chaotic) can be observed depending on the initial conditions. As a control parameter α decreases to the transition value α_0 the burst duration can be as long as $|\ln(\alpha - \alpha_0)|$. Realization of this mechanism predicts that there exist critical control parameter values for which the system exhibits intermittency so that the system can generate a long train of bursts before it finally settles down into periodic spiking. This intermittency is also a consequence of Smale horseshoe dynamics.

The dynamic feature of this bifurcation is bi-stability which means the co-existence of a pair of attractors separated in the phase space. The bifurcation of a saddle-node periodic orbit with homoclinic orbits provides a perfect explanation for this phenomenon. Namely, after the saddle-node periodic orbit splits into a stable periodic orbit and a saddle one in the phase space, the stable manifold of the latter can separate the attraction basin of the bursting from that of a stable periodic orbit representing the tonic spiking. Furthermore, we identify a physiologically plausible parameter in the neuron model (2.1) (introduced below) that can control duration of a burst, the time interval between the first and last spikes in the burst.

The second mechanism describing a reversible and continuous transition between spiking and bursting activities in neuron models is based on a codimension-one bifurcation known as the blue sky catastrophe [15, 16, 17]. Rigorous proofs and three scenarios of the blue sky catastrophe in singularly perturbed systems can be found in [18]. In [17] this bifurcation was shown to occur in a modified Hindmarsh-Rose model. The geometry of the bifurcation is illustrated in Fig. 2.

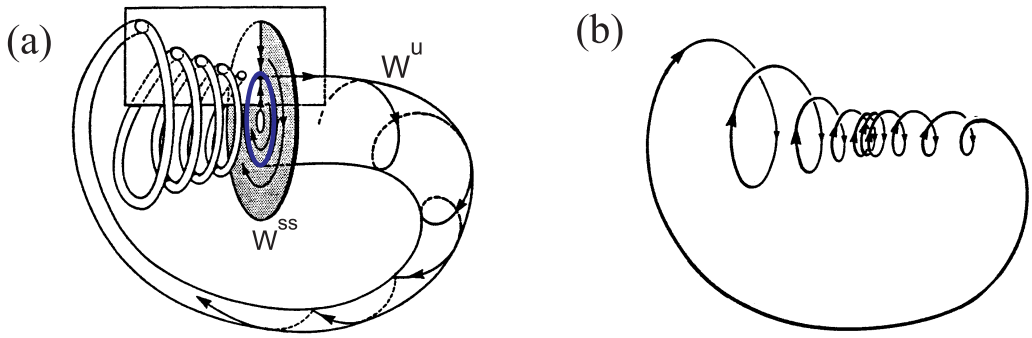

Fig. 2. Geometry of the blue sky bifurcation (a) resulting in the appearance of a large amplitude stable periodic orbit of an infinitesimally long period (b).

At the bifurcation, there exists a saddle-node periodic orbit L_{sn} whose two-dimensional unstable manifold W^u returns to the periodic orbit making infinitely many rotations in the node (attracting) region from the left of the strongly stable manifold W^{ss}. As a control parameter passes the critical value, the saddle-node periodic orbit disappears. Endowed with the property of a strong contraction in the transverse direction, the blue sky bifurcation results in the appearance of a new stable periodic orbit of infinite period and length. The infinite period of the periodic bursting is due to the slow passage of of the phase point through the "phantom" of the disappeared saddle-node orbit.

We study these transitions in a model of a pharmacologically isolated heartbeat interneuron from the medicinal leech. The activity of these neurons is well described under normal and pharmacologically modified conditions by mathematical models [19, 20] developed in accordance with Hodgkin-Huxley formalism [21]. Below we introduce the model of a single leech neuron. Then we develop a general geometrical framework for the analysis of periodic solutions of slow-fast dynamical systems. It allows us to give a general phenomenological description for the Lukyanov-Shilnikov bifurcation of a saddle-node periodic orbit with non-central homoclinics and the blue sky catastrophe in our systems. Throughout the presentation we draw parallels between the phenomenological description and the accurate numerical bifurcation analysis of the model of the single leech neuron. The developed technique is applicable to a broad class of neuron models. Our results make feasible predictions for future experimental studies.

2. Neuron model

A bursting regime reflects complexity in the dynamics of various membrane ionic currents, operating at different time scales. The ionic currents are commonly quantified through voltage-clamp experiments and modeled according to a formalism introduced by Hodgkin and Huxley [21]. A complete neuron model, including all currents identified experimentally, is rather complex for thorough studies. The relatively small number of neurons in invertebrate nervous systems and possibility to identify most of them from preparation to preparation, all make these identifiable neurons attractive for the dynamical systems analysis. Here we exploit identified oscillator interneurons that are part of the leech heartbeat central pattern generator.

When isolated pharmacologically from the rest of the network these neurons show autonomous bursting behavior [19]. In these neurons, eight voltage-dependent ionic currents have been well identified and characterized, see [22, 23] and references therein. Classified by their ionic specificity, these currents are separated in four groups. The first group consists of two sodium currents: a fast sodium current (I_{Na}) and a persistent sodium current (I_{NaP}). The second group consists of three potassium currents: a delayed rectifier-like potassium current (I_{K1}), a persistent potassium current (I_{K2}) and a fast transient potassium (I_{Ka}). The third group consists of two low-threshold calcium currents: one rapidly (I_{CaF}) and one slowly inactivating (I_{CaS}). The last group consists of a single current, carried by both sodium and potassium: a hyperpolarization-activated current (I_h). All these currents except, for the fast sodium current, were quantified in voltage clamp experiments [23]. The model equations for I_{Na} current were borrowed from the original work by Hodgkin and Huxley adjusted for leech kinetics. None of these currents is dependent on the intracellular concentration of any particular ion. A canonical model of a single neuron has been constructed and tuned to reproduce experimentally observed behaviors [23]. It consists of fourteen ordinary differential equations running at multiple time scales which vary from a few milliseconds through seconds. As alluded to above a comprehensive analysis of this model would be quite difficult and challenging.

Blockade of groups of currents in living heart interneurons simplifies neuronal dynamics, and elicits characteristic behaviors. These characteristic behaviors present interesting phenomena for study from the perspective of the theory of dynamical systems. One of the commonly observed characteristic behaviors is observed under blockade of Ca^{2+} currents. In leech neurons, application of divalent ions like Co^{2+}, which block Ca^{2+} currents, along with partial block of outward currents, elicits slow plateau-like oscillations with a period up to 60 seconds and plateau duration up to 20 seconds. This phenomenon persists after a blockade of I_h.

Previously, in our modeling studies [19], we addressed the question of how these slow temporal characteristics are produced by a system with dynamics based on much faster time scales (time constants of the ionic currents involved do not exceed one second). We derived a simplified neuron model by taking into account that the experimental conditions eliminated or reduced the contribution of certain currents to the dynamics of the neuron. This simplified model, based on the dynamics of I_{Na} and I_{K2} currents, is described as a system of three differential equations. We showed that the classical model of the transient Na^+ current is sufficient for the generation of long plateau behavior due to the properties of a window current (a transient Na^+ current can be a persistent "window" current in a certain range of membrane potential values). The simplified model (2.1) can also produce slow plateau-like oscillations with a sufficiently long plateau phase.

To bring the 14D canonical model developed in [23] in accordance with the experimental conditions described above, we remove from the model the equations and terms describing blocked currents: I_{CaF}, I_{CaS}, and I_h. For simplicity, we assume that the partial block of outward currents completely removes I_{K1}, as well as I_{KA}, whereas it reduces I_{K2}. The current I_{NaP} is ignored for simplicity. The resulting model described in [19] reads as follows:

$$\begin{aligned} C\mathrm{V}' &= -(\bar{\mathrm{g}}_{\mathrm{K2}}\ \mathrm{m}_{\mathrm{K2}}^2(\mathrm{V}-\mathrm{E}_{\mathrm{K}}) + \mathrm{g}_{\mathrm{l}}\ (\mathrm{V}-\mathrm{E}_{\mathrm{l}}) + \\ &\quad \bar{\mathrm{g}}_{\mathrm{Na}} f(-150, 0.0305, \mathrm{V})^3 \mathrm{h}_{\mathrm{Na}}(\mathrm{V}-\mathrm{E}_{\mathrm{Na}})), \\ \mathrm{m}'_{\mathrm{K2}} &= \frac{f(-83, 0.018 + \mathrm{V}_{\mathrm{K2}}^{\mathrm{shift}}, \mathrm{V}) - \mathrm{m}_{\mathrm{K2}}}{\tau_{\mathrm{K2}}}, \\ \mathrm{h}'_{\mathrm{Na}} &= \frac{f(500, 0.03391, \mathrm{V}) - \mathrm{h}_{\mathrm{Na}}}{\tau_{\mathrm{Na}}}, \end{aligned} \tag{2.1}$$

where the variables V, m_{K2}, and h_{Na} are the membrane potential, activation of I_{K2} and inactivation of I_{Na}, respectively. The parameters are: C is the membrane capacitance, $\bar{g}_{K2}$ is the maximum conductance of I_{K2}; E_K and E_{Na} are the reversal potentials of K^+ and Na^+, respectively; $\bar{g}_{Na}$ is

the maximal conductance of I_{Na}; g_l and E_l are the conductance and reversal potential of the leak current, respectively; τ_{K2} and τ_{Na} are the time constants of activation of I_{K2} and inactivation of I_{Na}, respectively; V_{K2}^{shift} is the shift of the membrane potential of half-inactivation of I_{K2} from its canonical value; f is a Boltzman function: $f(x,y,z) = 1/(1+e^{x(y+z)})$. The values of the parameters used in this study are $C = 0.5$ nF, $\bar{g}_{K2} = 30$ nS, $E_K = -0.07$ V, $E_{Na} = 0.045$ V, $\bar{g}_{Na} = 200$ nS, $g_l = 8$ nS, $E_l = -0.046$ V, $\tau_{K2} = 0.9$ sec and $\tau_{Na} = 0.0405$ sec. We use V_{K2}^{shift} as a bifurcation parameter.

One of the features of the model (2.1) is the bi-stability where stable tonic spiking co-exists with the bursting mode, as shown in Fig. 3.

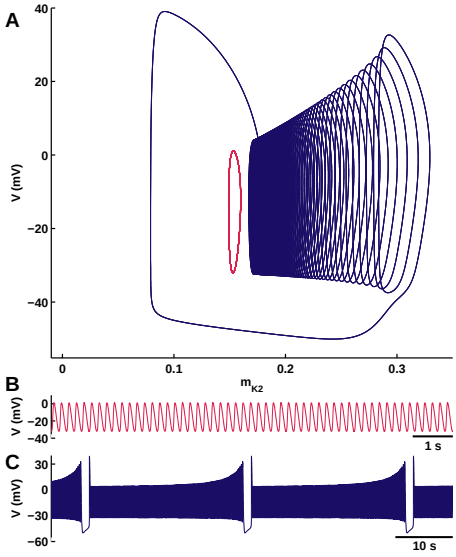

Fig. 3. Co-existence of spiking and bursting modes in the model (2.1) in the (m_{K2}, V)-projection for $V_{K2}^{shift} = -0.02598$ V. Initial conditions leading to tonic spiking and bursting are $(V, m_{K2}, h_{Na}) = (0.0, 0.164, 0.08)$ and $(0.0, 0.165, 0.08)$, respectively. The small round periodic orbit in (A) corresponds to the tonic-spikes shown in (B); the larger, bursting cycle corresponds to the waveform shown in (C). The topology of bursting is illustrated in Figs. 4.

3. Phenomenological description

In the model (2.1), the time constant of the activation of the current I_{K2} is more than 20 times larger that those of the membrane potential V and inactivation of the current I_{Na}. Hence, we identify m_{K2} as the slow phase variable and V and h_{Na} as the fast ones. This allows us to consider (2.1) as a singularly perturbed system written in the following form:

$$\dot{x} = F(x,z), \quad \dot{z} = \mu G(x,z,\alpha) \equiv \mu(g(x,\alpha) - z), \tag{3.1}$$

where $x \in \mathbb{R}^n$ $(n \geqslant 2)$ and $z \in \mathbb{R}^1$ are the fast and the slow phase space variables, respectively, α is a vector of control parameters, and $0 < \mu \ll 1$. Both functions F and G are considered smooth enough.

When $\mu = 0$, the fast and slow subsystems are decoupled. Now, the variable z can be viewed as a governing parameter for the fast subsystem. The function F is assumed to satisfy some conditions typical for the system (2.1). They are illustrated in Fig. 4(a). The first one is that, depending on z, the fast subsystem has either one or three hyperbolic equilibrium states.

The coordinates of equilibria of the fast system are found from the equation $F(x,z) = 0$ that defines a nullcline M_{eq} having a distinctive $\mathcal{Z}$-shape in projection onto the (z,x)-plane. The two

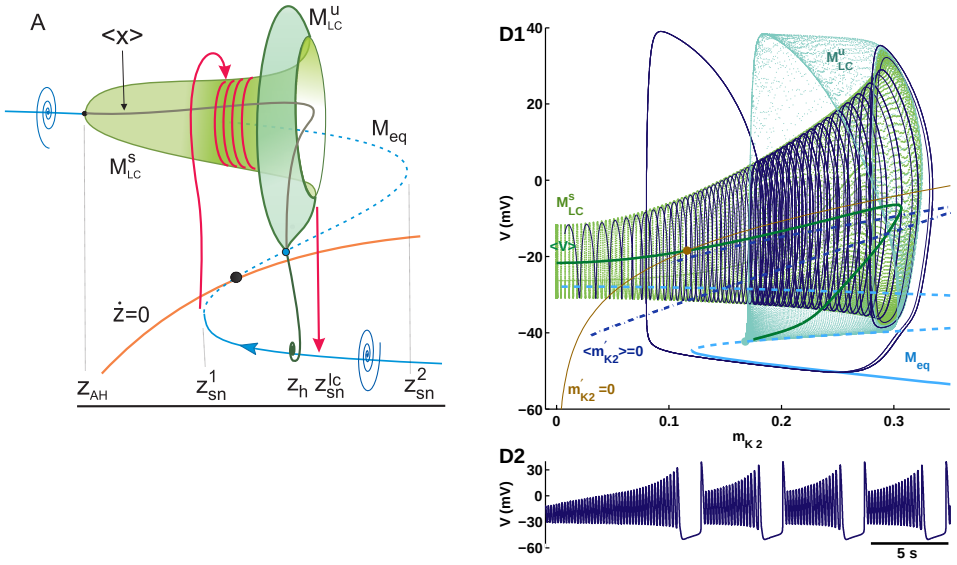

Fig. 4. (A) Geometry of bursting and bifurcation diagram of the fast subsystem in the (z, x)-extended phase plane. The curve M_{eq} consists of equilibrium points of the phase subsystem; its limit cycles span the surface M_{LC}. The curve $\langle x \rangle$ gives the average x-coordinate of the limit cycles. The nullcline $\dot{z} = 0$ crosses the unstable branch of M_{eq} at a single point corresponding to an unstable equilibrium state of the whole system. The arrowed curves outline the start and the end of a burst. (D) Geometry (D1) and the waveform (D2) of attracting bursting in the neuron model (2.1) at $V^{shift}_{K2} = -0.027$ V. The intersection point of the nullclines $m_{K2}{}' = 0$ and M_{eq} is the unstable equilibrium state of (2.1). The surface of M_{LC} is composed of the periodic orbits continued as the control parameter V^{shift}_{K2} is varied. There is no intersection between the average nullclines $\langle m_{K2}{}' \rangle = 0$ and $\langle V \rangle$. Accordingly, the trajectory shown coils around M_{LC} translating rightwards and converges to the bursting attractor.

turning points on M_{eq}, at z^1_{sn} and z^2_{sn}, correspond to the saddle-node bifurcations in the fast subsystem where a pair of equilibrium states coalesce. In the interval $z^1_{sn} < z < z^2_{sn}$, the system (3.1) has three equilibria. The middle segment of M_{eq} is comprised of saddle points. The upper and lower branches of the nullcline M_{eq} correspond to the depolarized and hyperpolarized states of a neuron, respectively. The hyperpolarized (solid) branch of M_{eq} is comprised of stable equilibria of the fast subsystem. It is supposed that the stable focus on the upper branch becomes unstable through a generic (codimension-one) Andronov-Hopf bifurcation when z passes the critical value $z_{AH} < z^1_{sn}$. There are the two types of this bifurcation: sub- and super-critical. In the subcritical case, the stable focus becomes unstable when a repelling limit cycle collapses into it. If there are no other equilibrium states before z_{AH}, then this unstable cycle may only originate from a saddle-node bifurcation of limit cycles. This saddle-node bifurcation also generates a stable limit cycle that surrounds both the equilibrium state and the unstable limit cycle. In the supercritical case, the stable limit cycle emerges from the focus as z increases through the bifurcational value z_{AH}. In either case, the supercritical Andronov-Hopf bifurcation or the saddle-node bifurcation for limit cycles gives rise to the surface M^s_{LC} comprised solely of the stable limit cycles of the fast subsystem. The subsequent evolution of the stable limit cycle as z increases further can develop in two different ways. For example, the branch M^s_{LC} may terminate at a homoclinic bifurcation of the saddle point on the middle branch of M_{eq}, like in [8, 9]; i.e., the stable limit cycle becomes a homoclinic orbit of the saddle point with the negative saddle value, which is a sum of the characteristic exponents of the saddle point of the fast subsystem. Oppositely, if the saddle value is positive, then another, unstable limit cycle bifurcates from the homoclinic orbit as z increases through z_h, thereby constituting the "unstable" surface M^u_{LC}. Hence, as z approaches the value z^{lc}_{sn}, the stable and the unstable limit cycles get closer and merge finally into a double one at z^{lc}_{sn}.

This value corresponds to a saddle-node bifurcation for the limit cycles in the fast subsystem. The last scenario makes the united surface $\mathrm{M_{LC}} = \mathrm{M^s_{LC}} \cup \mathrm{M^u_{LC}}$ look like it is turned inside out, see a sketch in Fig. 4 and its numerical reconstruction in Fig. 4(right).

After the stable limit cycle has vanished in the saddle-node bifurcation at $z > \mathrm{z^{lc}_{sn}}$, a neighboring phase point starts seeking another attractor, see Figs. 4 and 5(B). Such an attractor is the stable equilibrium state on the lower branch of $\mathrm{M_{eq}}$. As the parameter z is now decreased, the phase point follows this hyperpolarized branch towards the low knee point at $\mathrm{z^1_{sn}}$. The disappearance of this steady state attractor for $z < \mathrm{z^1_{sn}}$ triggers the phase point to switch back to the stable limit cycle on $\mathrm{M^s_{LC}}$.

Let us discuss the dynamics of the whole, singularly perturbed system (3.1) when $0 < \mu \ll 1$. Introduce another nullcline $\dot{z} = 0$, which is the surface given by $G(x, z, \alpha) = 0$, see Fig. 4. Let $\dot{z}$ be negative on $\mathrm{M_{eq}}$ wherever it is below the nullcline, be positive above it. An intersection point of this nullcline with the nullcline $\mathrm{M_{eq}}$ (where $\dot{x} = 0$) is the equilibrium state of the whole system. To make the system exhibit bursting behavior, let this equilibrium state be unstable, i.e. be on the unstable (dotted) branch of $\mathrm{M_{eq}}$. It follows from the works by Fenichel [24] that both surfaces, $\mathrm{M_{eq}}$ and $\mathrm{M_{LC}}$ will persist as invariant manifolds for small enough μ as well. Moreover, each remains μ-close to the original wherever it is normally hyperbolic (e.g. far from bifurcations). Therefore, the phase point of the whole system will follow the same path in the (z, x)-phase space. Namely, it translates slowly along the lower branch of $\mathrm{M_{eq}}$ leftward till the fold. Then, it makes a rapid, vertical jump up onto the surface $\mathrm{M_{LC}}$. Afterwards, it moves slowly rightward coiling around $\mathrm{M_{LC}}$. Having reached the edge of $\mathrm{M_{LC}}$ at $\mathrm{z^{lc}_{sn}}$, the phase point falls straight down onto $\mathrm{M_{eq}}$ to start a new cycle. Such trajectory behavior is associated with bursting in neuron models. The number of spikes in a burst is a number of complete revolutions of the phase point around $\mathrm{M_{LC}}$.

In the following section we discuss the conditions under which the system has a stable periodic orbit the surface $\mathrm{M^s_{LC}}$ that corresponds to tonic spiking. The presence of this orbit ma make $\mathrm{M^s_{LC}}$ non-transitive for slow coiling passages of the trajectories of the system.

3.1. Average nullclines and periodic orbits

The surface $\mathrm{M_{LC}}$ is composed of the limit cycles of the fast system at $\mu = 0$. Let us introduce the average value $\langle \mathrm{x} \rangle$ of the x-coordinate of such a limit cycle $\varphi(t;\, z)$ with period $T(z)$ at given z: $\langle x(z) \rangle = \dfrac{1}{T(z)} \int\limits_0^{T(z)} \varphi(t;\, z) dt$. By varying z, we define the corresponding continuous curve in the (z, x)-space, see Fig. 4. Evidently, it originates at the Andronov-Hopf bifurcation at $\mathrm{z_{AH}}$ and terminates at the homoclinic bifurcation at $\mathrm{z_h}$. The curve has a distinctive knee point at $\mathrm{z^{lc}_{sn}}$ corresponding to the saddle-node bifurcation of the stable and unstable limit cycles of the fast subsystem.

In the first approximation, the dynamics of the singularly perturbed system around $\mathrm{M^s_{LC}}$ is determined, by following "averaged" slow subsystem:

$$\dot{z} = \mu \langle G(z, \alpha) \rangle \equiv \frac{\mu}{T(z)} \int\limits_0^{T(z)} G(\varphi(t;\, z), z, \alpha)\; dt. \tag{3.2}$$

Hence, if $\langle G(z, \alpha) \rangle > 0$ within $\mathrm{z^1_{sn}} \leqslant z \leqslant \mathrm{z^{lc}_{sn}}$ at some α, then then surface $\mathrm{M_{LC}}$ is transitive for solutions of the system (3.1) that coil around $\mathrm{M_{LC}}$ slowly (at the rate of $\sim \mu$) translating rightward.

Let some z^0 between $\mathrm{z^1_{sn}}$ and $\mathrm{z^{lc}_{sn}}$ be a simple zero of the function $\langle G(z, \alpha) \rangle$ for some fixed α. This zero is also an equilibrium state of this averaged slow subsystem. This equilibrium state is stable if $\langle G(z^0, \alpha) \rangle_z < 0$, or unstable otherwise. Then, as follows from Pontryagin-Rodygin theory [25], every zero of $\langle G \rangle$ corresponds to a periodic orbit of the whole singularly perturbed system. The stability of the periodic orbit in the x-direction is determined by that of the corresponding limit cycle $\mathrm{M_{LC}}$ of the fast subsystem at the given z^0. Recall that the components $\mathrm{M^s_{LC}}$ and $\mathrm{M^u_{LC}}$ of $\mathrm{M_{LC}}$ are comprised of the stable and unstable limit cycle of the fast subsystem. Therefore, to study bifurcations of

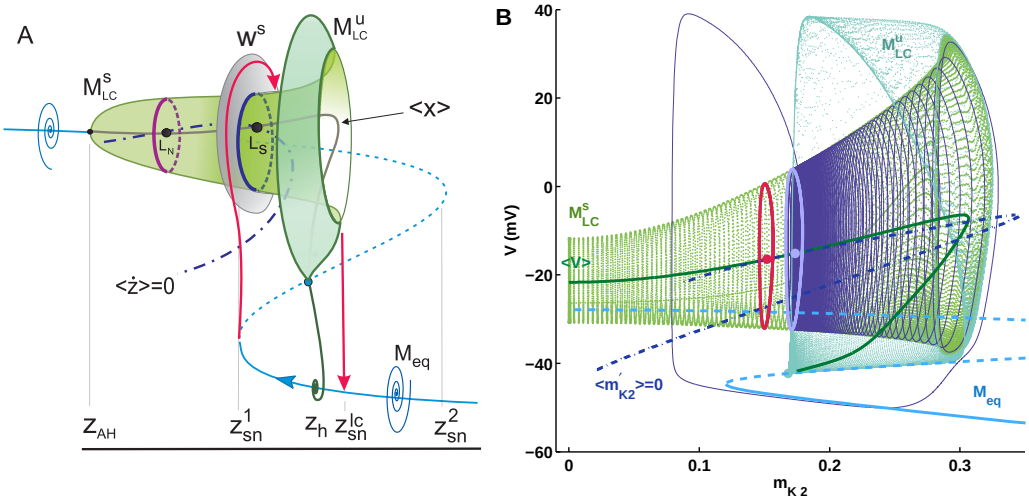

Fig. 5. (A) Intersection points of the average nullcline $\langle \mathrm{x} \rangle = 0$ with $\langle \mathrm{x} \rangle$ yield one stable, $\mathrm{L_n}$, and one saddle, $\mathrm{L_n}$, periodic orbits of the singularly perturbed system. The stable manifold $\mathrm{W^s}$ of the saddle periodic orbit $\mathrm{L_s}$ bounds the attraction basin of $\mathrm{L_n}$. This situation corresponds to Inset 4 in Fig. 6. (B) Intersection points of the nullclines $\langle \mathrm{m_{K2}}' \rangle = 0$ and $\langle \mathrm{V} \rangle$ yield the stable and saddle periodic orbits of the neuron system (2.1). The waveform of the bursting and tonic activities are shown in Fig. 3.

stable periodic orbits of the singularly perturbed system, we need to examine the upper branch of the curve $\langle \mathrm{x} \rangle$ corresponding to the stable component $\mathrm{M^s_{LC}}$.

Let us recall too that the function G is linear in z: $G(x, z, \alpha) = g(x, \alpha) - z$. Define an average nullcline $\langle \dot{z} \rangle = 0$ as the parametrically given curve $(z = \langle g(\zeta) \rangle, x = \langle x(\zeta) \rangle)$ with $\langle g(\zeta) \rangle = \frac{1}{T(\zeta)} \int\limits_0^{T(\zeta)} g(\varphi(t;\zeta), \alpha)\, dt$ and $\langle x(\zeta) \rangle = \frac{1}{T(\zeta)} \int\limits_0^{T(\zeta)} \varphi(t;\zeta)\, dt$. Any of its intersection point with the curve $\langle \mathrm{x} \rangle$ (comprised of pairs $(z, \langle x(z) \rangle)$) corresponds to a zero z^0 of $\langle G \rangle$, i.e. to a periodic orbit of our system. Note that if G is linear in both x and z, then the average nullcline $\langle \dot{z} \rangle = 0$ and the regular nullcline $\dot{z} = 0$ are the same curve. Evidently, this is not the general case. Furthermore, in contrast to the curve $\dot{\mathrm{z}} = 0$, which can be found analytically, the analysis of the location and the shape of the average nullcline $\langle \dot{z} \rangle = 0$ in the (z, x)-space requires numeric simulations. The corresponding average nullclines $\langle \mathrm{V} \rangle$ and $\langle \mathrm{m_{K2}}' \rangle = 0$ of the neuron model (2.1) are shown in Figs. 3(b), 7 and 8 for different values of the bifurcation parameter $\mathrm{V^{shift}_{K2}}$.

Next let us elaborate on how the average nullcline $\langle \dot{z} \rangle = 0$ may depend on the control parameter α in the slow equation of the system. Let α be introduced so that, the nullcline $\langle \mathrm{x} \rangle = 0$ crosses the upper, stable branch of the curve $\langle \mathrm{x} \rangle$ twice for some $\alpha > \alpha^*$. Then, these intersection points correspond to a pair of periodic orbits, one stable, $\mathrm{L_n}$, and one, $\mathrm{L_s}$, of the saddle type, see Figs. 5 and 7. By decreasing α, the distance between the orbit decreases, and when the average nullcline $\langle \mathrm{x} \rangle = 0$ has a tangency with the curve $\langle \mathrm{x} \rangle$ at some α^*, then the system possesses a saddle-node periodic orbit $\mathrm{L_{sn}}$, which vanishes for $\alpha < \alpha^*$, see Fig. 3(b). Additionally, we require that $\langle G(z^0, \alpha^*) \rangle_\alpha \neq 0$. If it is so, the distance between the bifurcating periodic orbits is evaluated as $\sqrt{\alpha - \alpha^*}$. When $\alpha < \alpha^*$, i.e. there are no periodic orbits on $\mathrm{M^s_{LC}}$ that becomes transitive, and then the neuron exhibits solely bursting activity.

4. Bi-stability and homoclinic saddle-node bifurcation

In order to reveal the origin of bi-stability, we continue to draw the parallels between the phenomenological description of bifurcations in the system (3.1) and the empirical studies of the neuron system (2.1).

We will also discuss a mechanism that gives rise the onset of chaos in the system. In both cases primary roles are played by the homoclinic bifurcations of the saddle and the saddle-node periodic orbits. Since the latter is the organizing center of our construction, let us start with its analysis first.

A spatial saddle-node periodic orbit has two unique manifolds, strongly stable W^{ss} and unstable W^s, in the particular case of $\mathbb{R}^3$ both are of dimension two [17]. The strongly stable manifold W^{ss} breaks a vicinity of the saddle-node periodic orbit L_{sn} into two regions: node and saddle. In the node region, the saddle-node periodic orbit is stable, i.e. a trajectory converges to it as time tends to $+\infty$. In contrast, L_{sn} is repelling in the saddle region, where it has the unstable manifold W^u comprised of orbits converging to the saddle-node in backward time. We are interested in the global behavior of this unstable manifold, more specifically, whether it can be homoclinic, i.e. bi-asymptotic to the saddle-node periodic orbit. Recurrent behavior of the solutions of the slow-fast systems depicted in Fig. 3 supports this assertion.

In this paper, we consider a particular situation where the unstable manifold W^u of the saddle-node periodic orbit comes back to the orbit along the strongly stable manifold W^{ss} of the saddle-node periodic orbit L_{sn}; see the sketch in Fig. 1.

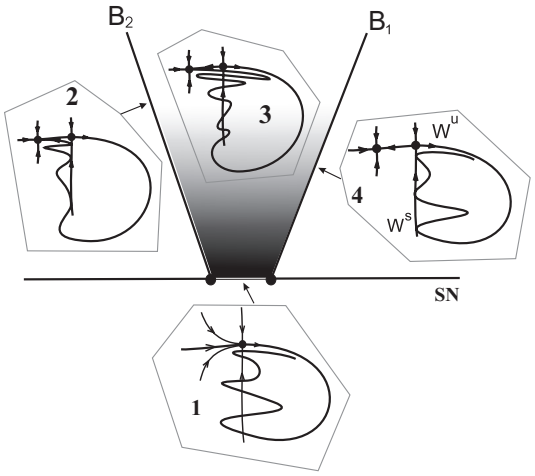

Fig. 6. There are three principal bifurcation curves in the unfolding for the Lukyanov-Shilnikov bifurcation of a saddle-node fixed point with non-central homoclinics (Inset 1 showing the Poincaré map). The two bifurcation curves, B_1 and B_2, which are the boundaries of the darkened sector, correspond to the very first (Inset 4) and last (Inset 2) homoclinic tangencies between the stable, W^s, and unstable, W^u, sets of the saddle fixed point. The complex hyperbolic structure existing in this sector, is due to transverse homoclinic crossings of these sets (Inset 3). This structure will persist also after the disappearance of the saddle-node point beneath the segment indicated on the bifurcation curve SN.

The case where W^u comes back from the node region making infinitely many revolutions, the so-called blue-sky catastrophe, will be discussed in the following section. Note that since an typical intersection of two surfaces in $\mathbb{R}^3$ is transverse, the presence noncentral homoclinic connections to the saddle-node does not raise the codimension of the bifurcation. This bifurcation was first introduced and studied by Lukyanov and Shilnikov [14]. Let us elaborate on its basic properties. The unfolding of the bifurcation is sketched in Fig. 6. This bifurcation is best described by using a two-dimensional Poincaré map which is defined on some cross-section transverse to the periodic orbits. The point where a periodic orbit hits the cross-section is a fixed point of the Poincaré map. The stability of each fixed point and the stability of the point corresponds to that of the periodic orbit. In the case of the saddle-node periodic orbit, there is a single fixed point of the fixed point of the saddle-node type with one multiplier equal +1. So, when the saddle-node periodic orbit L_{sn} splits into a stable, L_n,

and a saddle, L_s, periodic orbit, the corresponding saddle-node fixed point breaks into two points too: one stable and one fixed point of the saddle type. Let this occur above the corresponding bifurcation curve SN in Fig. 6.

Let α be a parameter controlling the distance between the fixed points so that there is no one when $\alpha > 0$. Let U be a small neighborhood containing the double fixed point with the homoclinic orbit, and let $\Omega_U(\alpha)$ denote the set of all trajectories lying entirely in U except for the stable orbit when $\alpha < 0$. Then we have the following two theorems.

Theorem 1 (Lukyanov–Shilnikov). *There exist a small neighborhood U of the origin and $\alpha_1 < 0$ such that for all $\alpha \in [\alpha_1, 0]$ the set $\Omega_U(\alpha)$ is homeomorphic with suspension over the Bernoulli subshift on two symbols.*

Theorem 2 (Lukyanov–Shilnikov). *There exists a neighborhood U, $\bar{\alpha} > 0$ and a partition of the interval $(0, \bar{\alpha}]$*

$$0 < \ldots < \alpha_{k+1+\bar{k}} < \alpha'_{k+1+\bar{k}} < \alpha_{k+\bar{k}} < \ldots < \alpha_{\bar{k}} = \bar{\alpha},$$

such that for $\alpha \in (\alpha_{k+1+\bar{k}}, \alpha_{k+\bar{k}}$ the set $\Omega_U(\alpha)$ contains an invariant subset $\Omega^k_U(\alpha)$ homeomorphic with the suspension over a Bernoulli subshift on $\bar{k} + k$ symbols, while $\Omega_U(\alpha)$ is homeomorphic with $\Omega^k_U(\alpha)$ for $\alpha \in (\alpha'_{k+1+\bar{k}}, \alpha_{k+\bar{k}})$. As $\alpha \to 0$ there arises an infinite set of bifurcation connected with the appearance of Smale horseshoes.

Because the saddle-node fixed point has non-central homoclinic orbits generated by transverse crossings of its unstable and strongly stable manifolds, it follows that after the splitting, the saddle point inherits the transverse homoclinic structure which implies that the system possesses a complex shift-dynamics above SN within the wedge bounded by two curves corresponding to the very first and last contacts between the stable and unstable manifolds of the saddle fixed point (periodic orbit) and below it. This dynamics is associated with the existence of the Smale horseshoes due to transverse intersections of the stable and unstable manifolds of the saddle-fixed point. As the fixed point disappears through the saddle-node bifurcation, the hyperbolic subset nevertheless persists so that the complex dynamics is still observed in the parameter region beneath the indicated sector. It is the main feature of saddle-node bifurcations of this kind.

Let us return to the description of the dynamics of the system (3.1). Above the curve SN, the stable L_n and saddle L_s periodic orbits co-exist on the tube M^s_{LC}. Of special interest here is the the right boundary B_1 (inset 4 in Fig. 6). This boundary corresponds to the first tangency between the stable W^s and unstable W^u manifolds of the saddle periodic orbit. To the right from B_1, the stable manifold W^s of the saddle orbit bounds the attraction basin of the stable periodic orbit. This situation corresponds to the co-existence of tonic spiking and bursting activities in the neuron, i.e. to bi-stability. Geometrically, the bi-stability in dynamics of the system (3.1) takes place, when the z^1_{sn}-coordinate of the left knee point on M_{eq} is on to right from the saddle periodic orbit L_s on the surface $M_{LC}{}^s$, see Fig. 5.

Let us return to consideration of the behavior of the solutions of the system 3.1 in the bi-stability sector between the bifurcation curves B_1 and B_2 in Inset 3 of Fig 6.

In our phenomenological description, we assume that the phase point makes momentarily vertical jumps between the slow motion surfaces M_{eq} and M_{LC}. In the neuron model, the appearance of these jumps may vary between projections of the phase space, compare for example Figs. 3 and 9(right), presenting the (m_{K2}, V)- and $(m_{K2}, -h_{Na})$-phase portraits, respectively.

The bi-stability in the neuron model (2.1) is illustrated in Figs. 5. Depending on initial condition, the system may generate tonic spiking, if the initial point is in the attraction domain of the stable periodic orbit, or it generates bursting activity. The saddle periodic orbit separates these attraction domains. The knowledge of the topology of the solutions of the slow-fast system gives a clear intuition how different kinds of stimulations may switch operation of the neuron between the tonic spiking and bursting modes. The influence of stimulation on the slow variable, m_{K2}, is apparently most

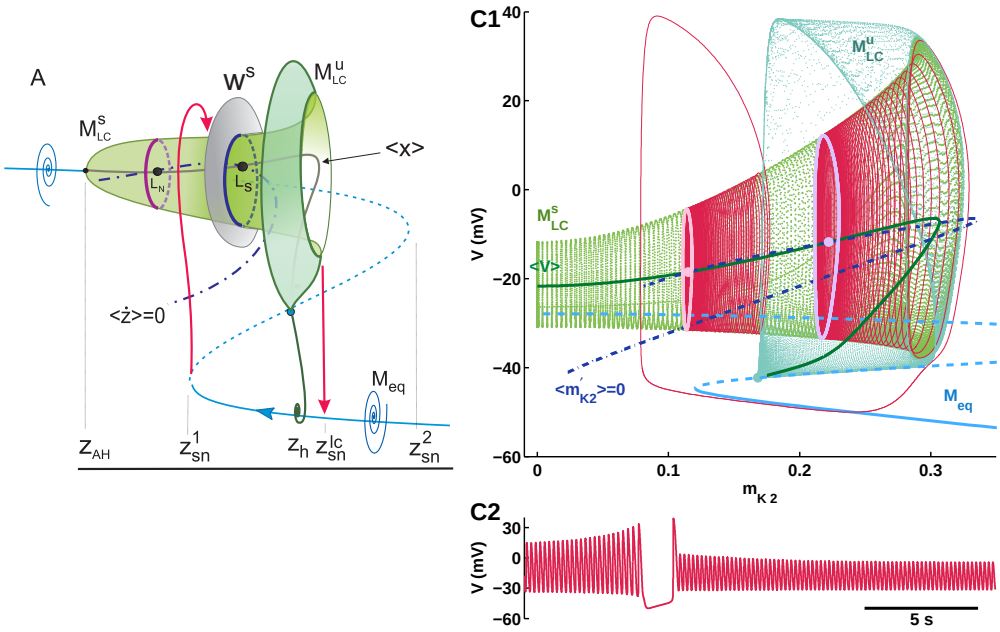

Fig. 7. The stable manifold of the saddle periodic orbit no longer separates the basing of the bursting from the basing of the stable periodic orbit corresponding to the tonic spiking activity at $V^{shift}_{K2} = -0.027$ V . This type of behavior takes place to the left of the bifurcation curve B_2 (Inset 2) in Fig. 6.

important. For the parameter regime presented in Figs. 5, if m_{K2} is chosen below 0.16, the tonic spiking is observed, while the bursting occurs for values exceeding a threshold 0.17, provided the same initial values for V and h_{Na}.

When the control parameter V^{shift}_{K2} is decreased, the stable and unstable periodic orbits move farther apart, so that the unstable manifold of the saddle orbit can no longer bound the attraction basin of the stable orbit where the phase point tends to as it jumps off the hyperpolarized phase of the bursting, as shown in Fig. 5. This situation corresponds to Inset 2 in Fig. 6 on the left of the curve B_2. Here, the neuron may only exhibit tonic spiking.

Observe that the duration of bursting phase may grow with no bound as the control parameter is moved toward the transition value between the regimes, while the interburst interval remains nearly constant, see Fig. 8. The estimate for the growth of the burst period is given by $T(z, \alpha^*)|\ln(\alpha - \alpha^*)|$, where α^* is a deviation of a control parameter from the boundary B_1 into the bursting region, and $T(z, \alpha^*)$ is the period of the limit cycle on the surface M_{LC} of the fast subsystem at the given z. Note also that the bursting behavior is not necessarily regular here but can be chaotic as well, especially when the phase point may pass close by the stable periodic orbit, see Fig. 9(right).

On the left of the boundary B_2, the bi-stability ends so that the tonic spiking becomes the dominant regime. For the model (3.1), this situation occurs when the left knee point at z^1_{sn} turns out to be to the left of the saddle periodic orbit L_s on M^s_{LC}. Any trajectory starting on the right of the stable manifold W^s of the saddle periodic orbit will get attracted to the stable one right after a single cycle of bursting, see Inset 2 in Fig. 6. The corresponding phase space portrait of the neuron system (2.1) is shown in Fig. 7.

The intermittency in the system takes place between the boundaries B_1 and B_2, as shown in Inset 3 in Fig. 6. Here, the system may generate a train of bursting before it starts firing continuous spikes. The exact number of bursts and duration of each burst in the train are impossible to predict. This is another consequence of the complex shift dynamics due to homoclinic wiggles pictured in Fig. 6 (inset 3). Figure 9 shows a chaotic train composed of four bursts. The width of the parameter interval corresponding to the intermittency is small in a singularly perturbed system with $|\mu| \ll 1$.

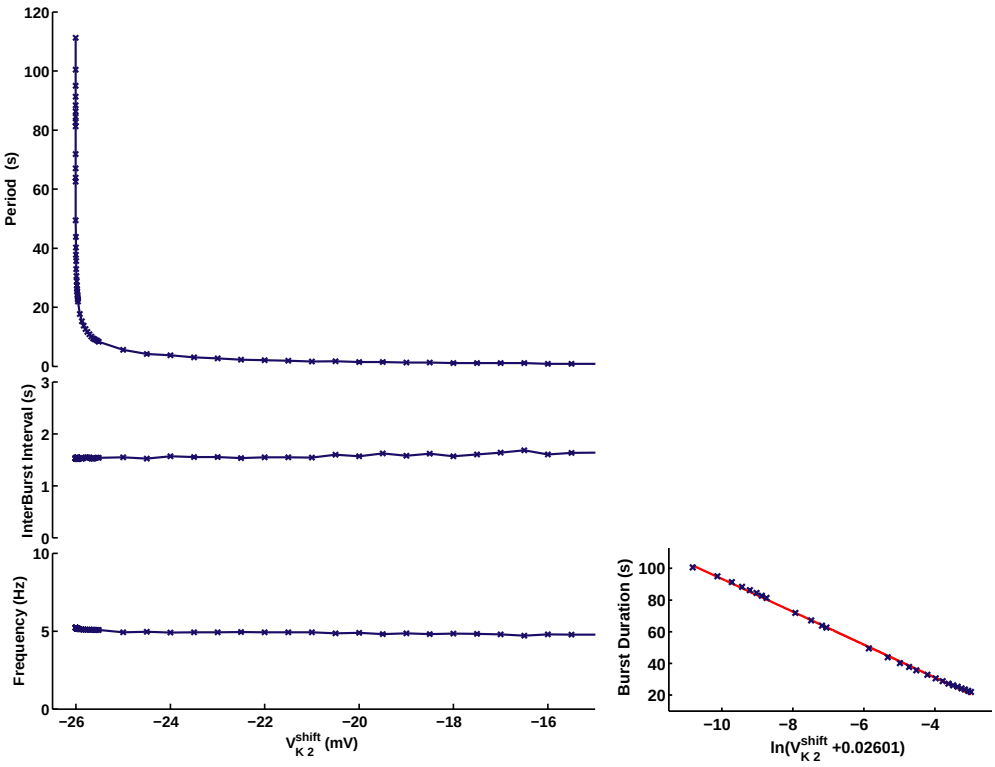

Fig. 8. (left) Temporal characteristics of bursting en route to spiking. The burst period (top chart) increases as $\sim |\ln(V^{shift}_{K2} + 0.2600866)|$. Interburst interval (middle) and frequency of spikes (bottom) remain almost constant. (right) Logarithmic fit of the dependence of the burst duration on the control parameter V^{shift}_{K2}. Note that the burst duration obeys the same law because the interburst interval hardly changes within the indicated parameter interval. The logarithmic fit of the burst duration in given in on the left chart.

Furthermore, it is proportional to the diameter of the tube of the unstable manifold W^u, which is shrinking while it gets back to the saddle-node periodic orbit, see the sketch in Fig. 1. Recall that the low hyperpolarized branch of M_{eq} is comprised of the stable equilibria of the fast subsystem. In virtue of Liouville's theorem, a low estimate for volume compression can be given by $e^{(\mathrm{divF}+\mu)\tau}$, with $\tau \simeq (z^{lc}_{sn} - z^{1}_{sn})/\mu$ and $\mathrm{divF} < 0$ on the low branch of M_{eq}. So, if μ is small, so is the diameter of the tube of the unstable manifold W^u and, hence, is the size of the intermittency interval in the parameter space. This makes this kind of intermittency transition hard to find in a singular perturbed system. On the other hand, its presence can serve as indirect evidence that the system does not run on multiple time scales.

5. Blue sky catastrophe

In this section we discuss another novel mechanism describing a reversible and continuous transition between spiking and bursting activities in neuron models. The geometry of the bifurcation in the singularly perturbed system (3.1) and the neuron model (2.1) is illustrated in Fig. 10. Recall from the introduction that we seek a saddle-node periodic orbit with the unstable manifold returning to the periodic orbit making infinitely many rotations in the node region. Besides the vector field is supposed to possess the property of a strong transverse contraction. If it is so, the blue sky bifurcation gives rise to a stable periodic orbit of infinite period and length. The infinite period of the periodic bursting is due to the slow passage of of the phase point through the "phantom" of the disappeared saddle-node orbit.

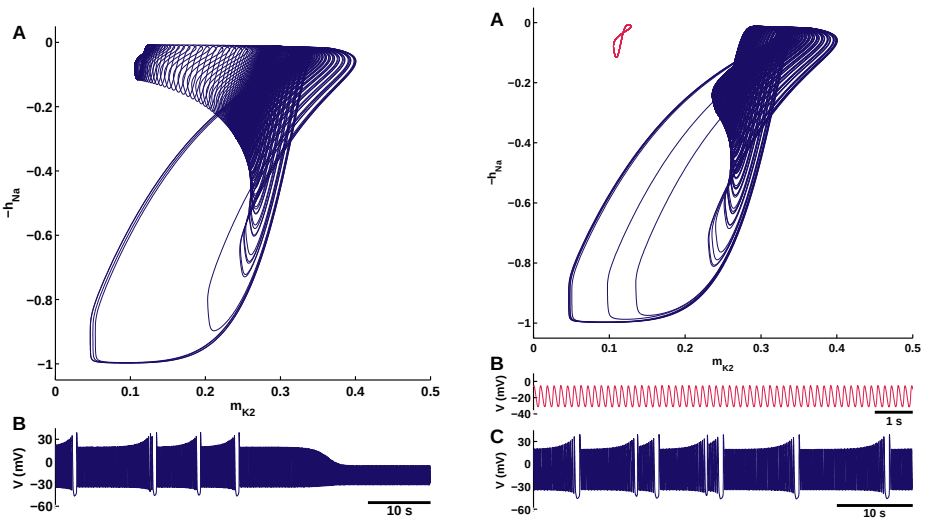

Fig. 9. (left) Intermittent transition to tonic spiking. A number of bursts are generated before the stable periodic orbit captures the phase point as illustrated in a projection to the $(-\mathrm{h_{Na}}, \mathrm{m_{K2}})$-phase plane (top) and as a voltage-time series (bottom) at $\mathrm{V_{K2}^{shift}} = 0.03367$ V. This intermittency corresponds to region (3) in Fig. 6. (right) Chaotic bursting at $\mathrm{V_{K2}^{shift}} = 0.0336709$ V presented in a projection on the $(-\mathrm{h_{Na}}, \mathrm{m_{K2}})$ plane and as a voltage-time series. Adjusting $\mathrm{V_{K2}^{shift}}$ regularizes bursting as shown on the left.

Suppose that the function $\langle G\rangle$ has a pair of zeros on the interval $[\mathrm{z_{sn}^1}; \mathrm{z_{sn}^{lc}}]$ at some $z_i^0(\alpha)$, $i = 1, 2$. It follows from Pontryagin-Rodygin' theory [25] that each zero corresponds to a periodic orbit of the whole, singularly perturbed system. Stability of a robust periodic orbit is determined by two factors. First, its stability in the x-space follows from the stability of the corresponding robust limit cycle in the phase space of the fast sub-system for the given $z_i^0(\alpha)$. Second, it is stable in z if $\partial\langle G\rangle/\partial z < 0$ at $z_i^0(\alpha)$, and unstable otherwise.

Let the distance between the zeros be controlled by a parameter α so that it vanishes at some $\alpha = \alpha_0$. Then, a plain saddle-node bifurcation occurs at α_0 provided that $\partial^2\langle G\rangle/\partial z^2 \neq 0$ at the critical point, and hence the distance between points is evaluated as $\sim \sqrt{\alpha - \alpha_0}$.

Introduce next an averaged nullcline $\langle \dot z\rangle = 0$ as the graph defined by the following points $(\langle g\rangle; \langle x\rangle)$, where $\langle g(z,\alpha)\rangle = 1/T(z)\int_0^{T(z)} g(\varphi(t;z),\alpha)dt$; note that both components depend parametrically on z. If for given α this nullcline $\langle \dot z\rangle = 0$ crosses transversally the curve $\langle x\rangle$, then the z-coordinate of such an intersection point is evidently a simple zero of the function $\langle G(z)\rangle$, i.e. equals z_i^0. Recall that $\langle G(z_i^0)\rangle$=0 means $\langle g(z,\alpha)\rangle - z_i^0 = 0$ as follows from (3.1). This observation lets one visualize effectively the locations of the periodic orbits in the phase space of the singularly perturbed system, as well as determine their possible bifurcations. The approach is used for the neuron model (2.1) to create partition of its phase space shown in Fig. 10b, with $\langle \mathrm{V}\rangle$ and $\langle \mathrm{m_{K2}}'\rangle = 0$ standing for the corresponding nullclines.

Variations of the parameter α translate the curve $\langle \dot z\rangle = 0$ in the (z, x)-space, so that one may make both curves have a quadratic tangency for some $\alpha = \alpha_0$. This saddle-node bifurcation for the periodic orbits constitutes the first component in the blue-sky catastrophe in slow-fast systems. A plain saddle-node periodic orbit in R^n, $n \geqslant 3$, has two unique manifolds. The strongly stable manifold $\mathrm{W^{ss}}$ divides locally a vicinity of the saddle-node orbit into two regions: node and saddle, see Fig. 10a. In the node region, a trajectory is attracted to the periodic orbit. In the saddle region, the periodic orbit is repelling. The unstable manifold $\mathrm{W^u}$ consists of the trajectories which are attracted to the saddle-node periodic orbit in backward time. As for the forward time, a trajectory on $\mathrm{W^u}$ follows the path of the bursting regime, i.e. moves leftwards along the lower, hyperpolarized branch of $\mathrm{M_{eq}}$, and provided that $\mathrm{z_{sn}} < \mathrm{z_{bs}}$, returns to the saddle-node orbit from the left, as seen in Fig. 10b. Thus,

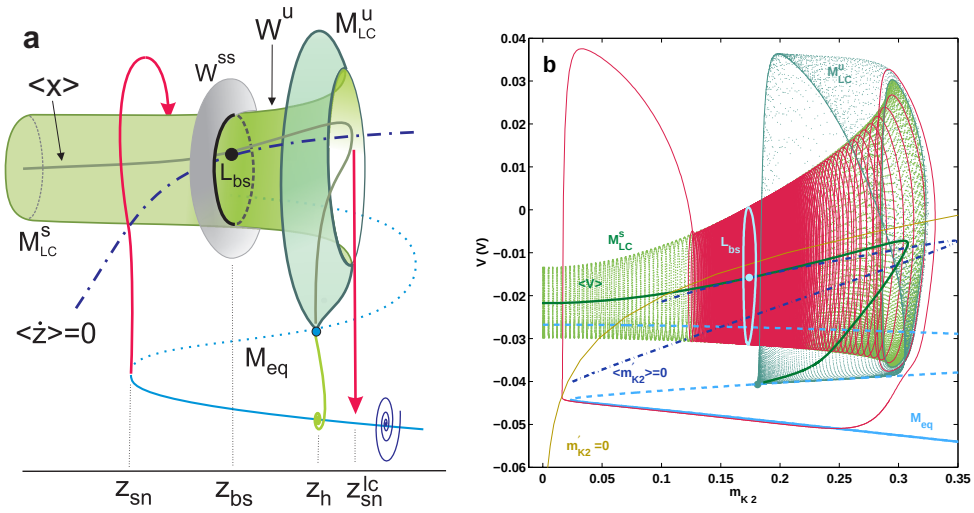

Fig. 10. Phenomenological sketch (a) and the matching numerical portrait (b) of the neuron model (2.1) at the blue sky catastrophe. A saddle-node periodic orbit L_{bs} is depicted in (a) for the slow-fast system (2) in the (z, x)-phase space combined with the bifurcation diagram of its fast subsystem, (b) for the neuron system (1) in $(\mathrm{m_{K2}}, \mathrm{V})$-phase space for $\mathrm{V^s_{K2}} = 24.5$ mV. The blue z-shaped line, $\mathrm{M_{eq}}$, consists of the equilibrium states of the fast subsystem (dotted and solid segments represent unstable and stable ones). The point of its intersection with the regular nullcline $\mathrm{m_{K2}}' = 0$ is a single equilibrium state of (2.1). The green cylinder-shaped surface $\mathrm{M_{LC}} = \mathrm{M^s_{LC}} \cup \mathrm{M^u_{LC}}$ is comprised of the stable and unstable limit cycles of the fast subsystem. The line $\langle \mathrm{x} \rangle$ shows the dependence of the x-coordinate of the limit cycle averaged over its period on z, and $\langle \mathrm{V} \rangle$ vs. $\mathrm{m_{K2}}$ in (b). The dashed, blue line is the average nullcline $\langle \dot{z} \rangle = 0$ in (a) and $\langle \mathrm{m_{K2}}' \rangle = 0$ in (b). The contact point between $\langle \mathrm{V} \rangle$ and $\langle \mathrm{m_{K2}}' \rangle = 0$ corresponds to the saddle-node periodic orbit, $\mathrm{L_{bs}}$. The gray disk $\mathrm{W^{ss}}$ in (a) is its strongly stable manifold. The part of $\mathrm{M^s_{LC}}$ to the right of $\mathrm{L_{bs}}$ is locally the unstable manifold, $\mathrm{W^u}$ of the saddle-node periodic orbit. In (a), the red line outlines rapid transitions of the phase point between the hyperpolarized phase and tonic spiking phase of bursting. In (b), the red curve represents a trajectory homoclinic to $\mathrm{L_{bs}}$. This trajectory transforms into a closed periodic orbit representing bursting as parameter $\mathrm{V^s_{K2}}$ passes a bifurcation value and $\mathrm{L_{bs}}$ disappears.

globally the unstable manifold $\mathrm{W^u}$ is homoclinic to the periodic orbit, which is the second component of the blue sky catastrophe.

When the bifurcation parameter $\alpha > \alpha_0$, i.e. the average nullcline is lifted up, the saddle-node orbit decouples into stable and unstable ones. The former corresponds to tonic spiking in a neuron. When the nullcline is lowered, the saddle-node periodic orbit vanishes and gives rise to a new stable periodic orbit of a large period and amplitude. This orbit could be considered as consisting of two phases, silent (interburst) and spiking. The spiking phase represents a burst. This orbit corresponds to bursting in a neuron. The burst duration, the time interval that the phase point needs to pass by the phantom of the saddle-node, is estimated as $1/\sqrt{\alpha - \alpha_0}$. Hence, by adjusting the deviation of the parameter α from the critical value α_0 one may control the burst duration without changing the interburst interval, see Figs. 2 and 3. Thus, a continuous transition from the bursting into tonic spiking is achieved by a single parameter variation. This transition is demonstrated in the neuron model (2.1) in Fig. 11. The parameter $\mathrm{V^s_{K2}}$ plays the role of the control parameter α. Variations of $\mathrm{V^s_{K2}}$ determine the position of the corresponding average null-cline $\langle \mathrm{m_{K2}}' \rangle = 0$. As the parameter $\mathrm{V^s_{K2}}$ approaches critical value 24.25 mV the duration of bursting interval increases with no bound as predicted. The standard deviation of the period of bursting oscillations remains zero while the parameter is varied thereby confirming that the observed regime is indeed represented by a stable periodic orbit. If one changes the parameter backwards, then the system will regain the round, stable periodic orbit corresponding to spiking, so that the segment of $\mathrm{M_{LC}}$ between $\sim \mathrm{m_{K2}} \in [0.02; 0.32]$ of

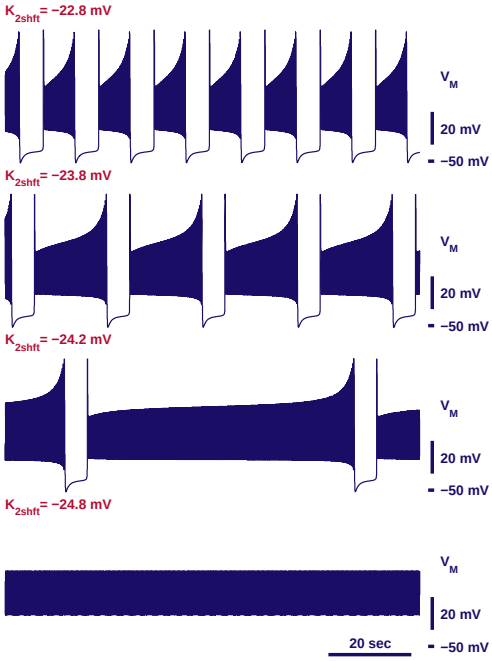

Fig. 11. Examples of oscillatory waveforms generated by the neuron model (1) for decreasing values of the bifurcation parameter V^s_{K2}. The bursting regime (three top traces) is continuously transformed into tonic spiking (bottom trace). The burst duration increases as V^s_{K2} approaches the blue-sky bifurcation's value ($V^s_{K2} = = 24.25$mV).

the bursting phase, becomes no longer transitive (Fig. 10b). This kind of the boundary between the regimes can be called *safe* following the terminology introduced in [17].

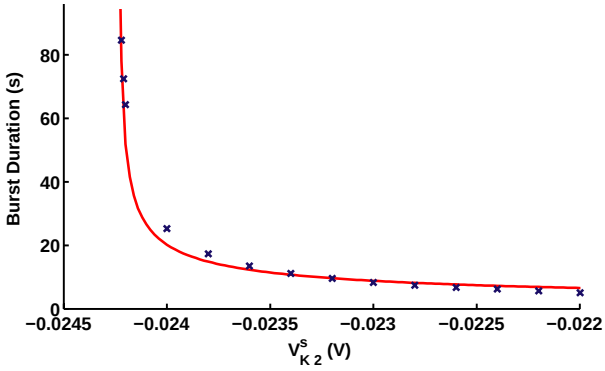

Fig. 12. Dependence of the period of bursting on the control parameter V^s_{K2}. The numerically obtained points are marked by ×-s. The approximating curve is given by $0.31/\sqrt{|(V^s_{K2} + 24.25)|}$, where 24.25 mV is the critical value of the transition.

Asymptotic estimates of the dependence of temporal characteristics of bursting on the control parameter are in a good agreement with the numerically obtained data for the neuron model (Fig. 12). The burst duration is well approximated by the following estimate $\sim 1/\sqrt{V^s_{K2} + 24.25}$, where $V^s_{K2} < 0$ and is presented in mV. The period of bursting suffices the same estimate, because the interburst interval remains almost constant. As the control parameter changes from -22.20 mV to -24.25 mV the interburst interval decreases from 6.16 s to 5.51 s, compared to the burst duration growing from 5.66 s to 957 s. The spike frequency remains constant ~ 5.5 Hz which is a physiologically observable value. It is worth noticing that the number of spikes in a burst is directly proportional to the duration of the burst.

6. Conclusion

We propose two new general scenarios of transitions between tonic spiking and bursting. The first mechanism also explains bi-stability in the system, where bursting mode co-exists with tonic spiking so that either mode can be attained by appropriate choice of initial conditions. The core of the mechanism is based on a bifurcation of codimension one for a saddle-node periodic orbit with non-central homoclinic orbits. We identified this scenario in a leech neuron model (2.1). For the first time this bifurcation has been shown to occur in a autonomous model describing the dynamics of a physical entity. We argue that it is typical for slow-fast systems based on the Hodgkin-Huxley formalism. Since the key bifurcation of the scenario is of codimension one, it may be revealed in electrophysiological experiments. The signatures of the key bifurcation are (1) coexistence of tonic spiking and bursting; (2) smooth transition between the two regimes; (3) logarithmic growth of the burst duration *en route* toward to tonic spiking; (4) chaotic intermittency of transient bursting turning into tonic spiking.

The second mechanism of the continuous transition between tonic spiking and bursting regimes in a model of a pharmacologically treated leech heartbeat interneuron is based on the bifurcation of the blue sky catastrophe. It is also is generic for a broad class of neuronal models utilizing Hodgkin-Huxley formalism. Its key features are (a) the bursting activity is periodic; (b) the period grows without a bound and obeys a universal law $T \sim 1/\sqrt{\alpha - \alpha_0}$ as the control parameter α decreases to the critical value α_0; (c) beyond α_0 the system exhibits periodic spiking; (d) the transition is reversible as the parameter is changed backward. These features describe a biophysically plausible control mechanism for regulation of bursting activity. Our study is the first application of this novel bifurcation to realistic neuron models and to any physical system in general.

In this work we have employed the technique of Pontryagin's averaging and made it easy to comprehend in the computational neuroscience context. Our description is not restricted to the given three-dimensional neuron model and holds for higher dimensions as well. The developed geometrical framework for an averaging method can be applied to studies of singularly perturbed systems of the given type. It constitutes a powerful tool for effective detection and bifurcation analysis of periodic orbits in neuron models.

7. Acknowledgment

The numeric analysis of system (2.1) utilized the software package CONTENT [26]. A.S. acknowledges the RFBR grants No. 02-01-00273 and No. 01-01-00975. G.C. was supported in part by NIH grants NS43098. We also appreciate a GSU internal research team grant and GSU Brain and Behaviors program support.

References

[1] *R. Bertram, M. J. Butte, T. Kiemel, A. Sherman.* Topological and phenomenologial classication of bursting oscillations. Bull. Math. Biol. 1995. V. 57. №3. P. 413–439.

[2] *J. Guckenheimer, S. Gueron, R. M. Harris-Warrick.* Mapping the dynamics of a bursting neuron. Philos. Trans. Royal Soc. Lond. Biol. Sci. 1993. V. 341. P. 345–359.

[3] *E. Izhikevich.* Neural excitability, spiking and bursting. Bifurcation and Chaos. 2000. V. 10. №6. P. 1171–1266.

[4] *J. Rinzel.* Bursting oscillations in an excitable membrane model, in Ordinary and Partial Differential Equations. Lecture Notes in Mathematics. 1985. V. 1151. P. 304.

[5] *V. N. Belykh, I. V. Belykh, M. Colding-Joregensen, E. Mosekilde.* Homoclinic bifurcations leading to bursting oscillations in cell models. Eur. Phys. J. E. 2000. V. 3. P. 205.

[6] *C. R. Laing, B. Doiron, A. Longtin, L. Noonan, R. W. Turner, L. Maler.* Type I burst excitability. J. Comput. Neuroscience. 2003. V. 14. P. 329.

[7] *B. Doiron, C. Laing, A. Longtin.* Ghostbursting: A novel neuronal burst mechanism. Comp. Neuroscience. 2002. V. 12. P. 5.

[8] *D. Terman.* The transition from bursting to continuous spiking in an excitable membrane model. J. Nonlinear science. 1992. V. 2. P. 133–182.

[9] *X. J. Wang.* Genesis of bursting oscillations in the Hindmarsh-Rose model and homoclinicity to a chaotic saddle. Physica D. 1993. V. 62. P. 263–274.

[10] *M. Bazhenov, I. Timofeev, M. Steriade, T. J. Sejnowski.* Spiking-bursting activity in the thalamic reticular nucleus initiates sequences of spindle oscillations in thalamic networks. J. Neurophysiology. 2000. V. 84. P. 1076–1087.

[11] *B. Deng, G. Hines.* Food chain chaos due to Shilnikov's orbit. Chaos. 2002. V. 12. №3. P. 533–538.

[12] *A. Shilnikov, G. Cymbalyuk.* Transition between tonic-spiking and bursting in a neuron model via the blue-sky catastrophe. Submitted to Phys. Review Letter. 2004.

[13] *A. Shilnikov, R. Colabrese, G. Cymbalyuk.* Mechanism of bi-stability: tonic spiking and bursting in a neuron model. Submitted to Phys. Review E. 2004.

[14] *V. Lukyanov, L. Shilnikov.* On some bifurcations of dynamical systems with homoclinic structures. Soviet Math. Dokl. 1978. V. 19. №6. P. 1314–1318.

[15] *L. P. Shilnikov, D. V. Turaev.* On simple bifurcations leading to hyperbolic attractors. Comput. Math. Appl. 1997. V. 34. P. 441–457.

[16] *L. Shilnikov, D. Turaev.* A new simple bifurcation of a periodic orbit of blue sky catastrophe type. In Methods of qualitative theory of differential equations and related topics. Amer. Math. Soc. Transl., II Ser. 2000. V. 200. P. 165–188.

[17] *L. Shilnikov, A. Shilnikov, D. Turaev, L. Chua.* Methods qualitative theory in nonlinear dynamics. Volumes I and II. World Scientific. 1998 and 2001.

[18] *A. Shilnikov, L. Shilnikov, D. Turaev.* Blue sky catastrophe in singularly perturbed systems. Moscow Math. Journal (in press). 2004. V. 4.

[19] *G. S. Cymbalyuk, R. L. Calabrese.* A model of slow plateau-like oscillations based upon the fast Na+ current in a window mode. Neurocomputing. 2001. V. 38–40. P. 159-166.

[20] *G. S. Cymbalyuk, Q. Gaudry, M. A. Masino, R. L. Calabrese.* Bursting in leech heart interneurons: cell autonomous and network based mechanisms. J. Neuroscience. 2002. V. 22. P. 10580–10592.

[21] *A. L. Hodgkin, A. F. Huxley.* A quantitative description of membrane current and its application to conduction and excitation in nerve. J. Physiol. 1952. V. 117. P. 500–544.

[22] *C. A. Opdyke, R. L. Calabrese.* A persistent sodium current contributes to oscillatory activity in heart interneurons of the medicinal leech. J. Comp. Physiol. 1994. V. 175. P. 781–789.

[23] *A. Hill, J. Lu, M. Masino, O. Olsen, R. L. Calabrese.* A model of a segmental oscillator in the leech heartbeat neuronal network. J. Comput. Neuroscience. 2001. V. 10. P. 281–302.

[24] *N. Fenichel.* Geometric singular perturbation theory for ordinary differential equations. J. Diff. Eq. 1979. V. 31. P. 53–98.

[25] *L. S. Pontryagin, L. V. Rodygin.* Periodic solution of a system of ordinary differential equations with a small parameter in the terms containing derivatives. Sov. Math. Dokl. 1960. V. 1. P. 611–614.

[26] CONTENT is available at ftp://ftp.cwi.nl/pub/CONTENT.